

# Structural Analysis on Iron-Based Superconductor Pr1111 System with Oxygen Deficiency and Flourine Substitution

Katsuaki KODAMA<sup>1,2</sup>, Motoyuki ISHIKADO<sup>1,2</sup>, Fumitaka ESAKA<sup>3</sup>, Akira IYO<sup>2,4</sup>, Hiroshi EISAKI<sup>2,4</sup>, and Shin-ichi SHAMOTO<sup>1,2</sup>

<sup>1</sup>Quantum Beam Science Directorate, Japan Atomic Energy Agency, Tokai, Ibaraki 319-1195, Japan

<sup>2</sup>JST, Transformative Research-Project on Iron Pnictides (TRIP), Tokyo 102-0075, Japan

<sup>3</sup>Nuclear Science and Engineering Directorate, Japan Atomic Energy Agency, Tokai, Ibaraki 319-1195, Japan

<sup>4</sup>Nanoelectronics Research Institute, National Institute of Advanced Industrial Science and Technology, Tsukuba, Ibaraki 305-8562, Japan

(Received August 24, 2018)

We have performed structural analyses on iron-based superconductors,  $\text{PrFeAsO}_{1-y}$  and  $\text{PrFeAsO}_{1-x}\text{F}_x$ , systematically, by means of Rietveld method on neutron powder diffraction data. The shifts of iron ion valence from +2,  $\delta$ , are accurately determined from the occupancies of O and  $\text{O}_{1-x}\text{F}_x$  sites obtained by the Rietveld analysis and F-concentration obtained by secondary ion-microprobe mass spectrometry.  $T_c$ - $\delta$  curve of  $\text{PrFeAsO}_{1-y}$  is different from the curve of  $\text{PrFeAsO}_{1-x}\text{F}_x$ , indicating that  $\delta$  is not a principal parameter for  $T_c$  in so-called 1111 system. Structural parameters of the FeAs layers, for example, As-Fe-As bond angle and As-height from Fe layer, are different between both systems with similar  $\delta$ -values. Their parent compounds are also found to have different structural parameters, possibly due to the different synthetic conditions. These results suggest that the difference of structural parameters of FeAs layer is the origin of the discrepancy of  $T_c$ - $\delta$  curves of both systems and the  $T_c$ -value in the 1111 system is sensitive to the structural parameters. It may be attribute to an energy balance of the conducting bands contributing to the superconductivity.

KEYWORDS: iron-based superconductor, structural analysis, neutron diffraction

## 1. Introduction

Iron-based high- $T_c$  superconductor was first discovered by the partial substitution of flourine for oxygen in  $\text{LaFeAsO}$  which is a semimetal with an antiferromagnetic ordering.<sup>1)</sup> After this dicoverly, the series of  $\text{RFeAsO}_{1-x}\text{F}_x$  systems were synthesized and the superconducting transition temperature  $T_c$  reached up to about 55 K, where R is lanthanide elements.<sup>2-6)</sup> In these systems, the partial substitution of flourine for oxygen causes the change of the valence of iron ion from +2 to  $+(2-x)$ , resulting in so-called electron doping in the conducting bands which consist of Fe 3d orbitals. The electron doping is considered to cause the phase transition from antiferromagnetic state to superconducting state. In term of same idea,  $\text{RFeAsO}_{1-y}$  systems with the oxygen deficiency which also induces the electron doping are synthesized under high pressure and they also exhibit the superconductivity.<sup>7)</sup> Other compounds,  $\text{AFe}_2\text{As}_2$  with  $\text{A}=\text{Ba}$  or  $\text{Sr}$ , show the transition from antiferromagnetic ordering to superconducting state by the substitution of Co for Fe, which gives the excess 3d electrons.<sup>8)</sup>

In early stage of iron-based superconductor research, theoretical studies point out the role of electron doping. The 3d orbitals of Fe give the Fermi surface of a hole at  $\Gamma$ -point and the Fermi surface of an electron at M-point in reduced Brillouin zone.<sup>9)</sup> At non-doping, the nesting between Fermi surfaces at  $\Gamma$ - and M-points induces the spin density wave state (SDW) or antiferromagnetic ordering state. The electron doping suppresses the SDW, and, however, the nesting gives a dynamical spin fluctua-

tion which is considered to be origin of the superconductivity.<sup>10-13)</sup> The recent experimental results support the above theoretical picture. The inelastic neutron scattering measurements on  $\text{LaFeAsO}_{1-x}\text{F}_x$  with  $x=0.057$ , 0.082 and 0.157 indicate that the spin fluctuation observed in the sample with  $x=0.057$  and 0.082 which exhibit superconductivity, almost disappears in the sample with  $x=0.157$  in which the high- $T_c$  superconductivity is almost suppressed.<sup>14)</sup> It can be explained that the excess electron doping shrinks the hole Fermi surface at  $\Gamma$ -point. The shrinking of the hole Fermi surface is also observed by ARPES on over-doped  $\text{BaFe}_{2-x}\text{Co}_x\text{As}_2$  with  $x=0.3$  in which the superconductivity is almost suppressed.<sup>15)</sup> These results show the importance of the electron doping and/or the valence shift of Fe ion from +2 to the superconductivity.

However, several experimental results indicate that the valence shift of Fe ion is not solitary parameter to control the electronic state in the iron-based superconductors.  $T_c$  of  $\text{LaFeAsO}_{1-x}\text{F}_x$  system is highly suppressed around  $x=0.20$ , while the  $T_c$  of other lanthanide systems, for example, Ce and Pr, remain near maximum values at similar  $x$ -region.<sup>16-18)</sup> The Fe-valence at the boundary between antiferromagnetic ordering and superconducting phases in  $\text{LaFeAsO}_{1-x}\text{F}_x$  system is about +1.95 ( $x \sim 0.05$ ),<sup>1)</sup> very different from the value of about +1.6 of  $\text{PrFeAsO}_{1-y}$  system ( $y \sim 0.2$ ).<sup>7)</sup> On the other hand, early structural analysis on  $\text{RFeAsO}_{1-y}$  shows that the maximum  $T_c$  values of  $\text{RFeAsO}_{1-y}$  systems depend on As-Fe-As bond angles.<sup>19)</sup> Theoretical study indicates that an amplitude and  $Q$ -dependence of spin fluctua-

tion depend on the height of pnictogen ion, resulting in the difference of maximum  $T_c$ -values in  $R\text{FeAsO}_{1-y}$  systems.<sup>20)</sup> These results suggest that the structural parameters of FeAs layer are also important parameters for the electronic state in the iron-based superconductors. We have performed structural analyses on 1111 system with identical lanthanide element, Pr, in which superconductivities are induced by oxygen deficiency and fluorine substitution, in order to obtain information on the role of structural parameters to the electronic state and superconductivity.

## 2. Experiments

Powder samples of  $\text{PrFeAsO}_{1-y}$  and  $\text{PrFeAsO}_{1-x}\text{F}_x$  were prepared by following processes. Polycrystalline samples of  $\text{PrFeAsO}_{1-y}$  have been synthesized by high pressure method using belt-type-anvil apparatus. Powders of PrAs, Fe,  $\text{Fe}_2\text{O}_3$  were used as the starting materials for  $\text{PrFeAsO}_{1-y}$ . PrAs was obtained by reacting Pr powders and As grains at 500 °C for 10 hours and then 850 °C for 5 hours in an evacuated quartz tube. Mixed starting materials with their nominal compositions of  $\text{PrFeAsO}_{1-y}$  were sintered at 1000-1200 °C for 2 hours under a pressure of about 2 GPa using belt-type-anvil apparatus. The samples of about 1.8 g were prepared for neutron diffraction. Powder x-ray diffraction data show that obtained samples contain impurities of  $\text{Pr}_2\text{O}_3$ , FeAs and PrAs. The samples with nominal  $y$ -values larger than 0.2 are not used for the structural analysis because they contain the large amount of impurities. Powders of PrAs, Fe,  $\text{Fe}_2\text{O}_3$ , and  $\text{FeF}_2$  were used as starting materials for the synthesis of  $\text{PrFeAsO}_{1-x}\text{F}_x$ . The starting materials with nominal composition of  $\text{PrFeAsO}_{1-x}\text{F}_x$ , were mixed and sintered at 1100 °C for 10 hours in an evacuated quartz tube. The masses of samples for neutron diffraction are about 5 g. Powder x-ray diffraction data show that obtained samples contain only single  $\text{PrFeAsO}_{1-x}\text{F}_x$  phase. The ratios of oxygen and fluorine in the samples with finite  $x$  were determined by secondary ion-microprobe mass spectrometry (SIMS).

The  $T_c$  values are determined by the electrical resistivity measured by PPMS and the superconducting shielding diamagnetism measured by SQUID magnetometer.

Neutron powder diffraction measurements were performed at room temperature, using the high-resolution powder diffractometer HRPD (neutron wave length: 1.8234 Å, collimations: open (effective value of 35')-20'-6') installed in the reactor JRR-3 of JAEA. Diffraction data were collected with constant monitor counts and a step angle of 0.05 ° over the  $2\theta$  range of 10-162.4 °. These experimental conditions and the sample positions are completely common to all measurements. The powder samples were set in vanadium holders with diameters of 6 and 10 mm for  $\text{PrFeAsO}_{1-y}$  and  $\text{PrFeAsO}_{1-x}\text{F}_x$ , respectively.

## 3. Experimental Results

Temperature ( $T$ ) dependences of the resistivities of  $\text{PrFeAsO}_{1-y}$  are shown in Fig. 1(a). As shown in Fig. 1(a), the decrease of the resistivity of sample A-4 is some-

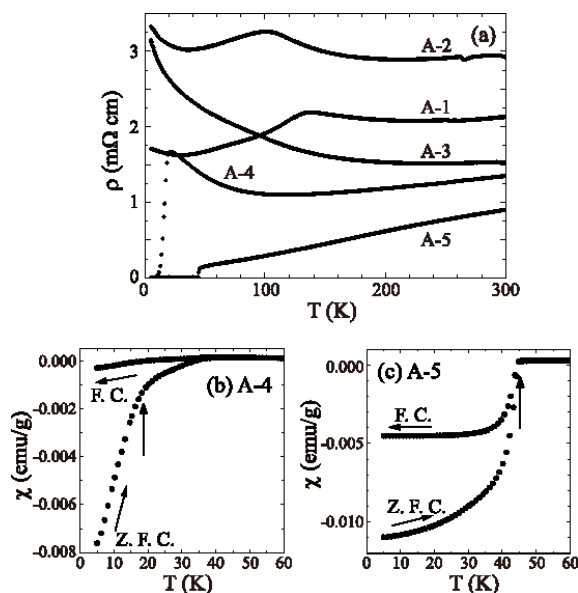


Fig. 1. (a) Temperature dependence of the electrical resistivities of  $\text{PrFeAsO}_{1-y}$  with  $y=0.0$  (sample A-1), 0.05 (A-2), 0.09 (A-3), 0.10 (A-4) and 0.20 (A-5). For all samples,  $y$  are nominal values. The magnetic susceptibilities are plotted for superconducting samples, A-4 (b) and A-5 (c). Signals in zero-field-cooling (Z. F. C. : superconducting shielding signal) and field-cooling (F. C. : Meissner signal) are shown. Vertical arrows show the onset temperature of superconducting shielding diamagnetism.

what broad at the superconducting transition. Here, we define the middle point between the onset of the resistivity drop and the zero-resistivity as the  $T_c$ -value estimated from the resistivity measurement,  $T_c^{\text{res}}$ .  $T$ -dependences of the magnetic susceptibilities of superconducting samples A-4 and A-5 are shown in Figs. 1(b) and 1(c). The onset temperature of the shielding is defined as  $T_c$ -value estimated from the shielding measurement,  $T_c^{\text{sh}}$ . For sample A-4, although the superconducting signal is observed at about 34 K, the signal is very small. Then we define  $T_c^{\text{sh}}=18$  K where clear drop of the signal is observed, as shown by vertical arrow. The values of  $T_c^{\text{sh}}$  almost correspond with the values of  $T_c^{\text{res}}$ . The resistivity of the sample with nominal  $y=0.09$  (sample A-3) does not exhibit superconductivity although the anomaly caused by the antiferromagnetic ordering and structural phase transition from the tetragonal to orthorhombic structure is not observed. The superconducting shielding diamagnetism is observed below about 16 K. However, because the volume fraction of the shielding signal is less than 1 % at about 4 K, this sample is regarded as non-superconducting sample.

Figure 2(a) shows the  $T$ -dependences of the resistivities of  $\text{PrFeAsO}_{1-x}\text{F}_x$ . In Figs 2(b), 2(c) and 2(d),  $T$ -dependences of the magnetic susceptibilities of superconducting samples B-2, B-3 and B-4 are shown, respectively. In the case of this system, the superconducting transitions observed in the resistivity and the shielding signal are sharp and the values of  $T_c^{\text{res}}$  almost correspond with the values of  $T_c^{\text{sh}}$ .

Figures 3(a) and 3(b) show the neutron powder diffraction patterns of the samples with nominal compositions

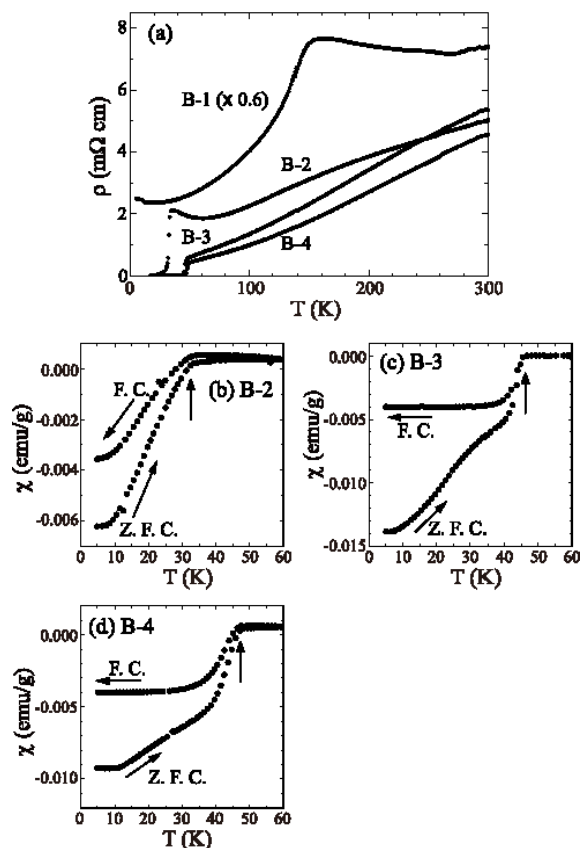


Fig. 2. (a) Temperature dependence of the electrical resistivities of  $\text{PrFeAsO}_{1-x}\text{F}_x$  with  $x=0.0$  (B-1), 0.05 (B-2), 0.10 (B-3) and 0.15 (B-4). For all samples,  $x$  are nominal values. The magnetic susceptibilities are plotted for superconducting samples, B-2 (b), B-3 (c) and B-4 (d). Signals in zero-field-cooling (Z. F. C. : superconducting shielding signal) and field-cooling (F. C. : Meissner signal) are shown. Vertical arrows show the onset temperature of superconducting shielding diamagnetism.

of  $\text{PrFeAsO}_{0.9}$  (sample A-4) and  $\text{PrFeAsO}_{0.9}\text{F}_{0.1}$  (sample B-3), as typical examples of the data on  $\text{PrFeAsO}_{1-y}$  and  $\text{PrFeAsO}_{1-x}\text{F}_x$ , respectively. The observed data are shown by crosses. Structural analyses on neutron powder diffraction data are performed by using the program RIETAN2000.<sup>21)</sup> The space group of  $P4/mmm$  is used. The data of  $\text{PrFeAsO}_{1-y}$  system are analyzed including  $\text{Pr}_2\text{O}_3$ , FeAs and PrAs as impurities, while the data of  $\text{PrFeAsO}_{1-x}\text{F}_x$  system are analyzed as single phase samples. The occupation factor of O and  $\text{O}_{1-x}\text{F}_x$  sites of  $\text{PrFeAsO}_{1-y}$  and  $\text{PrFeAsO}_{1-x}\text{F}_x$  are also refined, respectively, in order to determine the valence of Fe ion accurately. The obtained structural parameters of  $\text{PrFeAsO}_{1-y}$  and  $\text{PrFeAsO}_{1-x}\text{F}_x$  are shown in Tables I and II, respectively. Errors of the parameters shown in the tables are mathematical standard deviations obtained by Rietveld analysis. Mass fractions of the impurities in  $\text{PrFeAsO}_{1-y}$  are also shown in Table I. The diffraction patterns calculated by using refined parameters are shown in Figs. 3(a) and 3(b) by solid lines. The calculated lines can reproduce the observed data. In Table II, the accurate  $\text{O}_{1-x}\text{F}_x$  ratios of  $\text{PrFeAsO}_{1-x}\text{F}_x$  samples estimated by SIMS are also shown.

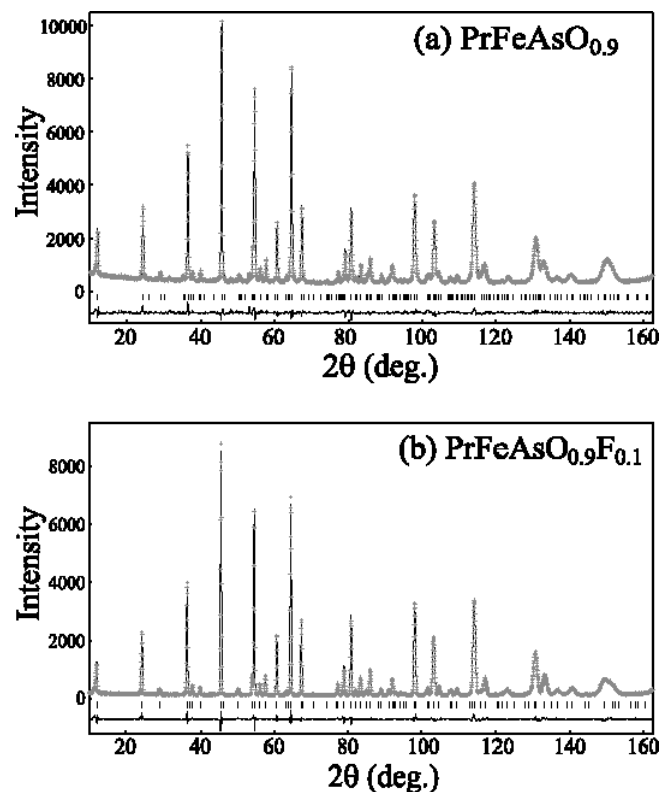


Fig. 3. Observed (crosses) and calculated (solid lines) neutron powder diffraction patterns of the samples with nominal compositions of  $\text{PrFeAsO}_{0.9}$  (a) and  $\text{PrFeAsO}_{0.9}\text{F}_{0.1}$  (b), respectively. Vertical bars show the calculated position of Bragg reflections including the impurities. The solid lines at the bottom of the figures are the differences between observed and calculated intensities

#### 4. Discussions

Now we can accurately estimate the shift of the Fe valence from +2,  $\delta$ , because the occupancies of O ( $\text{O}_{1-x}\text{F}_x$ ) site in  $\text{PrFeAsO}_{1-y}$  ( $\text{PrFeAsO}_{1-x}\text{F}_x$ ) and the ratio of  $\text{O}_{1-x}\text{F}_x$  in  $\text{PrFeAsO}_{1-x}\text{F}_x$  are accurately determined by neutron diffraction and SIMS measurements, respectively. We use the values of  $T_c^{\text{sh}}$  as  $T_c$ -values because  $T_c^{\text{sh}}$  almost correspond with  $T_c^{\text{res}}$ , as shown in previous section. In Fig. 4,  $T_c$  ( $T_c^{\text{sh}}$ ) of  $\text{PrFeAsO}_{1-y}$  and  $\text{PrFeAsO}_{1-x}\text{F}_x$  are plotted as functions of  $\delta$ , by closed circles and squares, respectively.  $T_c$ - $\delta$  curve of  $\text{PrFeAsO}_{1-y}$  obviously deviates from the curve of  $\text{PrFeAsO}_{1-x}\text{F}_x$ .  $T_c$ -value of  $\text{PrFeAsO}_{1-x}\text{F}_x$  increases against  $\delta$  rapidly than the value of  $\text{PrFeAsO}_{1-y}$ , and reaches the maximum  $T_c$ -value at  $\delta \sim 0.16$  while the  $T_c$ -value of  $\text{PrFeAsO}_{1-y}$  almost reaches the maximum at  $\delta \sim 0.29$ . These results indicate that the  $T_c$ -value is not determined only by  $\delta$ -value, at least, in so-called 1111 system even if the system consists of identical lanthanide element.

The lattice parameters  $a$  and  $c$  of  $\text{PrFeAsO}_{1-y}$  and  $\text{PrFeAsO}_{1-x}\text{F}_x$  are shown in Fig. 5 by the circles and squares, respectively. The superconducting and non-superconducting samples are shown by the closed and open symbols. The data are plotted as functions of  $\delta$ . At similar  $\delta$ -values, the values of  $a$  ( $c$ ) of  $\text{PrFeAsO}_{1-y}$

Table I. Structural parameters of  $\text{PrFeAsO}_{1-y}$  (space group  $P4/mmm$ ) determined by Rietveld analyses of neutron powder diffraction data at room temperature. Compositions of starting mixtures with  $y=0.0$ (a),  $y=0.05$ (b),  $y=0.09$ (c),  $y=0.10$ (d), and  $y=0.20$ (e).  $B$  is the isotropic displacement parameter.

Atom	Site	Occ.	$x$	$y$	$z$	$B$
(a) Sample A-1 (nominal $y=0.0$ , non-super.)						
$a=3.9861(2)$ , $c=8.6007(4)$ Å, $R_{\text{wp}} = 5.67\%$ , $R_{\text{wp}}/R_e = 1.40$						
Pr	2c	1	1/4	1/4	0.1387(4)	0.50(7)
Fe	2b	1	3/4	1/4	1/2	0.39(4)
As	2c	1	1/4	1/4	0.6566(3)	0.66(5)
O	2a	0.992(6)	3/4	1/4	0	0.28(6)
impurity : $\text{Pr}_2\text{O}_3$ 9.1 %, FeAs 8.6 %, PrAs 0.0 %						
(b) Sample A-2 (nominal $y=0.05$ , non-super.)						
$a=3.9854(2)$ , $c=8.5963(3)$ Å, $R_{\text{wp}} = 5.32\%$ , $R_{\text{wp}}/R_e = 1.33$						
Pr	2c	1	1/4	1/4	0.1394(4)	0.49(5)
Fe	2b	1	3/4	1/4	1/2	0.46(4)
As	2c	1	1/4	1/4	0.6562(2)	0.52(4)
O	2a	0.972(4)	3/4	1/4	0	0.26(5)
impurity : $\text{Pr}_2\text{O}_3$ 2.9 %, FeAs 2.3 %, PrAs 0.0 %						
(c) Sample A-3 (nominal $y=0.09$ , non-super.)						
$a=3.9861(1)$ , $c=8.5884(3)$ Å, $R_{\text{wp}} = 5.53\%$ , $R_{\text{wp}}/R_e = 1.15$						
Pr	2c	1	1/4	1/4	0.1390(3)	0.77(4)
Fe	2b	1	3/4	1/4	1/2	0.62(3)
As	2c	1	1/4	1/4	0.6564(2)	0.55(3)
O	2a	0.982(4)	3/4	1/4	0	0.44(4)
impurity : $\text{Pr}_2\text{O}_3$ 2.5 %, FeAs 1.8 %, PrAs 0.0 %						
(d) Sample A-4 (nominal $y=0.10$ , $T_c^{\text{res}}=15.8$ K, $T_c^{\text{sh}}=18$ K)						
$a=3.9798(1)$ , $c=8.5880(2)$ Å, $R_{\text{wp}} = 4.92\%$ , $R_{\text{wp}}/R_e = 1.27$						
Pr	2c	1	1/4	1/4	0.1400(3)	0.83(6)
Fe	2b	1	3/4	1/4	1/2	0.55(4)
As	2c	1	1/4	1/4	0.6574(2)	0.47(4)
O	2a	0.908(4)	3/4	1/4	0	0.13(5)
impurity : $\text{Pr}_2\text{O}_3$ 0.0 %, FeAs 2.7 %, PrAs 2.0 %						
(e) Sample A-5 (nominal $y=0.20$ , $T_c^{\text{res}}=45.3$ K, $T_c^{\text{sh}}=45$ K)						
$a=3.9709(2)$ , $c=8.5839(3)$ Å, $R_{\text{wp}} = 6.52\%$ , $R_{\text{wp}}/R_e = 1.54$						
Pr	2c	1	1/4	1/4	0.1423(3)	0.60(6)
Fe	2b	1	3/4	1/4	1/2	0.35(4)
As	2c	1	1/4	1/4	0.6579(3)	0.52(5)
O	2a	0.857(6)	3/4	1/4	0	0.50(6)
impurity : $\text{Pr}_2\text{O}_3$ 0.0 %, FeAs 2.8 %, PrAs 2.3 %						

are larger (smaller) than the values of  $\text{PrFeAsO}_{1-x}\text{F}_x$ . We note that even the parent compounds in both systems corresponding to the samples A-1 and B-1 have different lattice parameters although they have very similar composition of  $\text{PrFeAsO}_{0.992}$  and  $\text{PrFeAsO}_{0.987}$ . This discrepancy of the lattice parameters are caused by the different conditions of their syntheses as mentioned in §2. Because  $\text{PrFeAsO}_{1-y}$  system including the parent compound are synthesized under high pressure, the  $c$ -axis that PrO and FeAs layers are alternately stacked contracts relative to the  $c$ -axis of  $\text{PrFeAsO}_{1-x}\text{F}_x$  system.

The difference of lattice parameters naturally causes the difference of the structural parameters on FeAs layer which exhibits the superconductivity. The As-Fe-As bond angle,  $\alpha$ , defined in ref. 19 is the good indicator of the maximum value of  $T_c$  in  $\text{RFeAsO}_{1-y}$  systems.<sup>19)</sup> It is suggested that the  $T_c$ -value becomes maximum as the  $\alpha$ -value approaches  $109.47^\circ$  at which the FeAs<sub>4</sub> unit is a regular tetrahedron. On the other hand, theoret-

Table II. Structural parameters of  $\text{PrFeAsO}_{1-x}\text{F}_x$  (space group  $P4/mmm$ ) determined by Rietveld analyses of neutron powder diffraction data at room temperature. Compositions of starting mixtures with  $x=0.0$ (a),  $x=0.05$ (b),  $x=0.10$ (c), and  $x=0.15$ (d).  $\text{O}_{1-x}\text{F}_x$  ratio in the column are estimated by SIMS.

Atom	Site	Occ.	$x$	$y$	$z$	$B$
(a) Sample B-1 (nominal $x=0.0$ , non-super.)						
$a=3.9810(1)$ , $c=8.6230(2)$ Å, $R_{\text{wp}} = 6.44\%$ , $R_{\text{wp}}/R_e = 1.19$						
Pr	2c	1	1/4	1/4	0.1391(2)	0.78(4)
Fe	2b	1	3/4	1/4	1/2	0.58(3)
As	2c	1	1/4	1/4	0.6569(2)	0.51(3)
O	2a	0.987(4)	3/4	1/4	0	0.52(4)
(b) Sample B-2 (nominal $x=0.05$ , $T_c^{\text{res}}=32.2$ K, $T_c^{\text{sh}}=32$ K)						
$a=3.9773(1)$ , $c=8.6108(2)$ Å, $R_{\text{wp}} = 6.11\%$ , $R_{\text{wp}}/R_e = 1.14$						
Pr	2c	1	1/4	1/4	0.1409(2)	0.76(4)
Fe	2b	1	3/4	1/4	1/2	0.56(3)
As	2c	1	1/4	1/4	0.6571(2)	0.51(3)
$\text{O}_{0.945}\text{F}_{0.055}$	2a	0.986(4)	3/4	1/4	0	0.58(4)
(c) Sample B-3 (nominal $x=0.10$ , $T_c^{\text{res}}=46.1$ K, $T_c^{\text{sh}}=46$ K)						
$a=3.9749(1)$ , $c=8.6007(2)$ Å, $R_{\text{wp}} = 6.15\%$ , $R_{\text{wp}}/R_e = 1.13$						
Pr	2c	1	1/4	1/4	0.1430(2)	0.85(4)
Fe	2b	1	3/4	1/4	1/2	0.59(3)
As	2c	1	1/4	1/4	0.6577(2)	0.54(3)
$\text{O}_{0.878}\text{F}_{0.122}$	2a	0.990(4)	3/4	1/4	0	0.56(4)
(d) Sample B-4 (nominal $x=0.15$ , $T_c^{\text{res}}=48.7$ K, $T_c^{\text{sh}}=47$ K)						
$a=3.9711(1)$ , $c=8.5996(2)$ Å, $R_{\text{wp}} = 6.34\%$ , $R_{\text{wp}}/R_e = 1.19$						
Pr	2c	1	1/4	1/4	0.1443(3)	0.96(4)
Fe	2b	1	3/4	1/4	1/2	0.59(3)
As	2c	1	1/4	1/4	0.6583(2)	0.47(3)
$\text{O}_{0.868}\text{F}_{0.132}$	2a	0.985(4)	3/4	1/4	0	0.54(4)

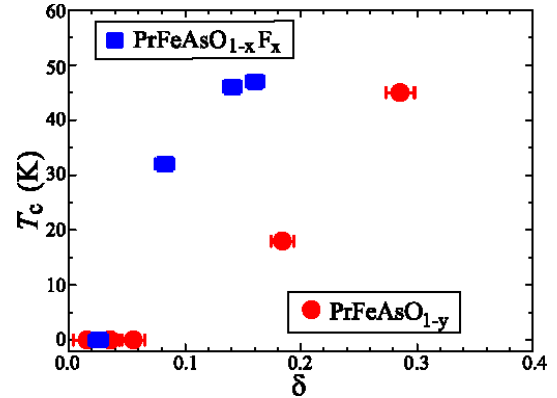


Fig. 4. (Color online)  $T_c$  of  $\text{PrFeAsO}_{1-y}$  and  $\text{PrFeAsO}_{1-x}\text{F}_x$  are plotted as a function of  $\delta$ , by closed circles and squares, respectively.

ical study suggests that the pnictogen height defined as  $(z_{\text{As}} - 0.5) \times c$  changes the spin fluctuation arising from Fermi surface nesting between  $\Gamma$  and M points which induces the  $s_{\pm}$  superconductivity. The spin fluctuation arising from the  $\Gamma$ -M Fermi surface nesting is enhanced with increasing the pnictogen height, resulting in the increase of  $T_c$ .<sup>20)</sup> Experimentally, it is suggested that  $T_c$  becomes maximum as the value of the pnictogen height approaches about  $1.38$  Å.<sup>22)</sup> Here we focus on these two structural parameters. In Fig. 6(a),  $\alpha$ -values of  $\text{PrFeAsO}_{1-y}$  and  $\text{PrFeAsO}_{1-x}\text{F}_x$  are plotted as func-



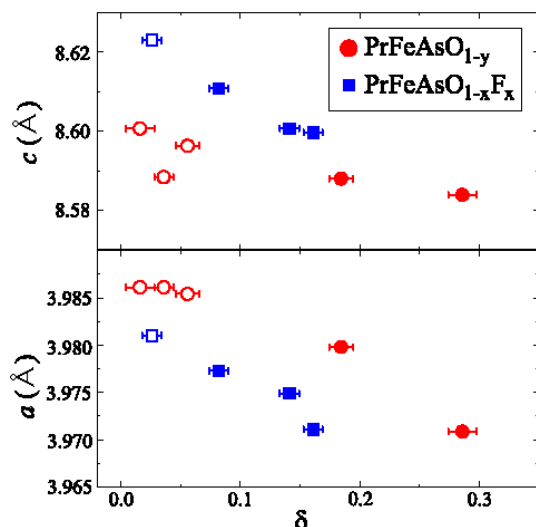


Fig. 5. (Color online) Lattice parameters of  $a$  (bottom panel) and  $c$  (top panel) of  $\text{PrFeAsO}_{1-y}$  and  $\text{PrFeAsO}_{1-x}\text{F}_x$  are plotted as a function of  $\delta$  by the circles and squares, respectively. The superconducting and non-superconducting samples are shown by the closed and open symbols.

tions of  $\delta$ . In both systems, the  $\alpha$ -values decrease with

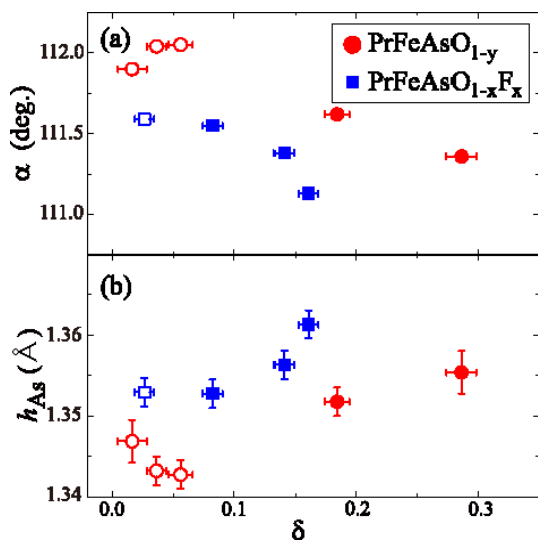


Fig. 6. (Color online) As-Fe-As bond angle,  $\alpha$ , defined in ref. 19 (a) and pnictogen height  $h_{\text{As}}$  defined in ref. 20 (b) of  $\text{PrFeAsO}_{1-y}$  and  $\text{PrFeAsO}_{1-x}\text{F}_x$  are plotted as functions of  $\delta$  by the circles and squares, respectively. The superconducting and non-superconducting samples are shown by the closed and open symbols.

increasing  $\delta$ , at least, consistent with the behavior in  $\text{RFeAsO}_{1-y}$  systems reported in ref. 19. The  $\alpha$ -values of  $\text{PrFeAsO}_{1-y}$  are larger than  $\alpha$  of  $\text{PrFeAsO}_{1-x}\text{F}_x$  at similar  $\delta$ -values, indicating that the FeAs layer of  $\text{PrFeAsO}_{1-y}$  is flatter than the layer of  $\text{PrFeAsO}_{1-x}\text{F}_x$  as expected from the relation of the lattice parameters between both systems shown in Fig. 5. In  $\text{PrFeAsO}_{1-x}\text{F}_x$ ,  $\alpha$  reaches the minimum value which almost corresponds with the reported value,<sup>4,19,23</sup> at smaller  $\delta$  relative to the case of  $\text{PrFeAsO}_{1-y}$ . In Fig. 6(b), the pnictogen

heights,  $h_{\text{As}}$  of  $\text{PrFeAsO}_{1-y}$  and  $\text{PrFeAsO}_{1-x}\text{F}_x$  are plotted as functions of  $\delta$ . The  $h_{\text{As}}$ -values of  $\text{PrFeAsO}_{1-x}\text{F}_x$  are larger than  $h_{\text{As}}$  of  $\text{PrFeAsO}_{1-y}$  at similar  $\delta$ -values. These results indicate that the structural parameters of FeAs layer are obviously different between  $\text{PrFeAsO}_{1-y}$  and  $\text{PrFeAsO}_{1-x}\text{F}_x$ . Such difference of FeAs layer may give the difference of  $T_c$ - $\delta$  curves shown in Fig. 4.

The strong correlation between the crystal structure and the magnetism of Fe ion is pointed out by other experimental studies. For example, phonon energy contributed from FeAs layer is smaller than the energy obtained by the first principle calculation, and this discrepancy can be corrected by the calculation which takes the magnetic moment of Fe into account.<sup>24</sup> The amplitude of ordered magnetic moment in the parent compound depend on the pnictogen height.<sup>25</sup> As mentioned in §1, the correlation between the magnetism and the superconductivity is also pointed out. The theoretical studies on iron-based superconductors suggest that three  $3d$  orbitals,  $3d_{x^2-y^2}$ ,  $3d_{zx}$  and  $3d_{yz}$  orbitals form the Fermi surfaces and the spin fluctuation arising from the nesting between the different Fermi surfaces induces the superconductivity.<sup>12,26</sup> Based on such scenario, the superconductivity and/or the spin fluctuation arising from the Fermi surface nesting can be sensitive to the structural parameters of FeAs layer because the energy levels of three  $3d$  orbitals are changed by the structural parameters. Our results confirm the strong correlation among the structural parameters, the magnetism and the superconductivity in the iron-based superconductors.

Here, we note that the change of the lattice parameter  $c$  of  $\text{PrFeAsO}_{1-y}$  are not perfectly systematic for the change of  $\delta$ , as shown in Fig. 5. The lattice parameter  $c$  of  $\text{PrFeAsO}_{1-y}$  with  $\delta \sim 0.04$  corresponding to sample A-3 is obviously smaller than the values of other two non-superconducting samples. As a possible origin of such behavior, it is suggested that the crystal structure of  $\text{PrFeAsO}_{1-y}$  system is metastable, at least, at high temperature, because  $\text{PrFeAsO}_{1-y}$  system can be synthesized only under high pressure. If the system is metastable, the slight difference of the synthetic condition can cause the difference of structural parameters. In addition, the resistivity of the sample A-3 does not exhibit the anomaly caused by antiferromagnetic ordering and structural phase transition while the sample A-2 with larger  $\delta$ -value exhibits antiferromagnetic ordering and structural phase transition. Such non-systematic behavior to  $\delta$  in  $\text{PrFeAsO}_{1-y}$  system also indicates the strong correlation between the structural parameters and the electronic state in iron-based superconductors.

Finally, we plot the  $T_c$ -values of  $\text{PrFeAsO}_{1-y}$  and  $\text{PrFeAsO}_{1-x}\text{F}_x$  against above structural parameters,  $\alpha$  and  $h_{\text{As}}$ . In Figs. 7(a) and 7(b),  $\alpha$  and  $h_{\text{As}}$  dependences of  $T_c$  are shown, respectively. Note that, in ref. 19 and 22,  $T_c$ -values of many types of iron-based superconductors whose "carrier doping levels" are adjusted to maximum  $T_c$ , are plotted against the  $\alpha$  and  $h_{\text{As}}$ . On the other hand, we plot  $T_c$  against the  $\alpha$  and  $h_{\text{As}}$  from antiferromagnetic phase to superconducting phase only on Pr1111 systems with oxygen deficiency and fluorine substitution.

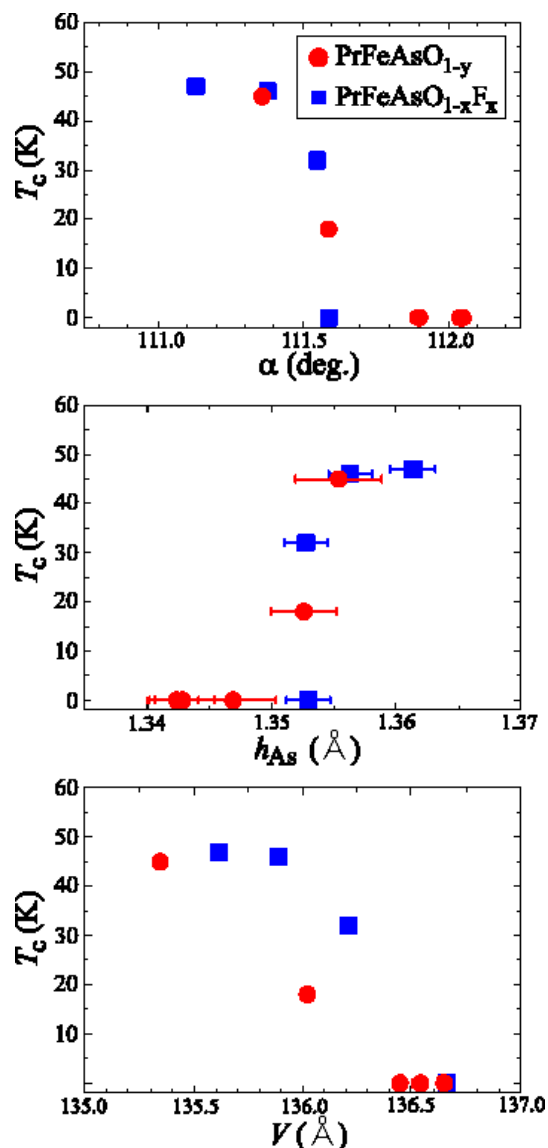


Fig. 7. (Color online)  $T_c$  of  $\text{PrFeAsO}_{1-y}$  and  $\text{PrFeAsO}_{1-x}\text{F}_x$  are plotted by closed circles and squares, respectively, as functions of  $\alpha$  (a),  $h_{\text{As}}$  (b), and volume of unit cell  $V$  (c).

$T_c$ -values of  $\text{PrFeAsO}_{1-y}$  and  $\text{PrFeAsO}_{1-x}\text{F}_x$  increase as  $\alpha$ -values approach the optimum value of  $109.47^\circ$ , qualitatively consistent with 1111 systems with other rare earth elements.<sup>19)</sup> Similar  $\alpha$ -dependence of  $T_c$  is also observed in hole doped 122 system.<sup>27)</sup>  $T_c$ -values of  $\text{PrFeAsO}_{1-y}$  and  $\text{PrFeAsO}_{1-x}\text{F}_x$  increase as  $h_{\text{As}}$ -values approach the optimum value of  $1.38$  Å. In  $\text{FeSe}_{1-x}\text{Te}_x$  system, the similar behaviors of  $\alpha$  and  $h_{\text{As}}$  are also observed, at least, in the  $x$  region from the antiferromagnetic ordering phase at  $x=1.0$  to the superconducting phase with maximum  $T_c$ -value at  $x=0.5$ .<sup>28, 29)</sup> These results suggest that the  $\alpha$  and  $h_{\text{As}}$  are important parameters for the appearance of the superconductivity although the relation between the  $\alpha$  and electronic state is not obvious. In addition, we also regard the volume-change as important. The  $T_c$ -value increases with decreasing unit cell volume as shown in Fig. 7(c). The similar behaviors are also observed in hole- and electron-doped 122 systems,<sup>27, 30)</sup> and  $\text{FeSe}_{1-x}\text{Te}_x$  system in the region of  $0.5 \leq x \leq 1.0$ .<sup>28)</sup> Simply consid-

ering the magneto-volume effect, a disappearance of the magnetic ordering in the sample with smaller volume is reasonable. However, the correlation between  $T_c$  and the unit cell volume is not obvious. Now we know that the  $T_c$ -value is sensitive to the structural parameters. The further systematic studies to reveal the correlation among the structural parameters, the electronic state and the superconductivity are necessary.

## 5. Summary

We have performed the Rietveld analyses on the neutron powder diffraction data of  $\text{PrFeAsO}_{1-y}$  and  $\text{PrFeAsO}_{1-x}\text{F}_x$  in which the superconductivities are induced by the oxygen deficiency and fluorine substitution, respectively. The  $T_c$ -values of both systems are not scaled by the valence shift of Fe ion,  $\delta$ , which is accurately determined by the Rietveld analysis. The structural parameters of FeAs layer are different between both systems including the parent compounds with the same composition. These results suggest that  $T_c$ -values of the iron-based superconductors are sensitive to the structural parameters of FeAs layer. Such sensitivity of  $T_c$  to the structural parameters may be due to the energy balance of  $3d$  orbitals contributing to the superconductivity which is affected by the structural parameters.

## Acknowledgment

The authors would like to thank M. Machida and H. Nakamura for their fruitful discussions and also N. Igawa for his help with the neutron diffraction measurements. This work is supported by a Grant-in-Aid for Specially Promoted Research 17001001 from the Ministry of Education, Culture, Sports, Science and Technology, Japan, and JST TRIP.

- 1) Y. Kamihara, T. Watanabe, M. Hirano, and H. Hosono : J. Am. Chem. Soc. **130** (2008) 3296.
- 2) G. F. Chen, Z. Li, D. Wu, G. Li, W. Z. Hu, J. Dong, P. Zheng, J. L. Luo, and N. L. Wang : Phys. Rev. Lett. **100** (2008) 247002.
- 3) G. F. Chen, Z. Li, D. Wu, J. Dong, G. Li, W. Z. Hu, P. Zheng, J. L. Luo, and N. L. Wang : Chin. Phys. Lett. **25** (2008) 2235.
- 4) Z. A. Ren, J. Yang, W. Lu, W. Yi, G. C. Che, X. L. Dong, L. L. Sun, Z.X. Zhao : Materials Research Innovations **12** (2008) 105.
- 5) X. H. Chen. and T. Wu, G. Wu, R. H. Liu, H. Chen and D. F. Fang : Nature **453** (2008) 761-762 .
- 6) R. H. Liu, G. Wu, T. Wu, D. F. Fang, H. Chen, S. Y. Li, K. Liu, Y. L. Xie, X. F. Wang, R. L. Yang, C. He, D. L. Feng and X. H. Chen : Phys. Rev. Lett. **101** (2008) 087001.
- 7) H. Kito, H. Eisaki, and A. Iyo, J. Phys. Soc. Jpn. **77** (2008) 063707.
- 8) A. S. Sefat, R. Jin, M. A. McGuire, B. C. Sales, D. J. Singh, and D. Mandrus : Phys. Rev. Lett. **101**, 117004 (2008).
- 9) D. J. Singh and M.-H. Du : Phys. Rev. Lett. **100** (2008) 237003.
- 10) I. I. Mazin, D. J. Singh, M. D. Johannes, and M. H. Du : Phys. Rev. Lett. **101** (2008) 057003.
- 11) V. Cvetkovic and Z. Tesanovic : Europhys. Lett. **85** (2009) 37002.
- 12) K. Kuroki, S. Onari, R. Arita, H. Usui, Y. Tanaka, H. Kontani, and H. Aoki : Phys. Rev. Lett. **101** (2008) 087004.
- 13) F. Ma and Z.-Y. Lu : Phys. Rev. B **78** (2008)033111.
- 14) S. Wakimoto, K. Kodama, M. Ishikado, M. Matsuda, R. Kajimoto, M. Arai, K. Kakurai, F. Esaka, A. Iyo, H. Kito, H. Eisaki, and S. Shamoto : J. Phys. Soc. Jpn. **79** (2010) 074715.

- 15) Y. Sekiba, T. Sato, K. Nakayama, K. Terashima, P. Richard, J. H. Bowen, H. Ding, Y.-M. Xu, L. J. Li, G. H. Cao, Z.-A. Xu, and T. Takahashi : *New J. Phys.* **11** (2009) 025020.
- 16) H. Luetkens, H.-H. Klauss, M. Kraken, F. J. Litterst, T. Dellmann, R. Klingeler, C. Hess, R. Khasanov, A. Amato, C. Baines, M. Kosmala, O. J. Schumann, M. Braden, J. Hamann-Borrero, N. Leps, A. Kondrat, G. Behr, J. Werner, and Büchner : *Nature Materials*, **8** (2009) 305.
- 17) J. Zhao, Q. Huang, Clarine De La Cruz, SHiliang Li, J. W. Lynn, Y. Chen, M. A. Green, G. F. Chen, G. Li, Z. Li, J. L. Luo, N. L. Wang, and Pengcheng Dai : *Nature Materials*, **7** (2008) 953.
- 18) C. R. Rotundu, D. T. Keane, B. Freelon, S. D. Wilson, A. Kim, P. N. Valdivia, E. Bourret-Courchesne, and R. J. Birgeneau : *Phys. Rev. B* **80** (2009) 144517.
- 19) C.-H. Lee, A. Iyo, H. Eisaki, H. Kito, M. T. Fernandez-Diaz, T. Ito, K. Kihou, H. Matsuhata, M. Braden, and K. Yamada : *J. Phys. Soc. Jpn.*, **77** (2008) 083704.
- 20) K. Kuroki, H. Usui, S. Onari, R. Arita, and H. Aoki : *Phys. Rev. B* **79** (2009) 224511.
- 21) F. Izumi and T. Ikeda : *Mater. Sci. Forum*, **321-324** (2000) 198.
- 22) Y. Mizuguchi, Y. Hara, K. Deguchi, S. Tsuda, T. Yamaguchi, K. Takeda, H. Kotegawa, H. Tou, and Y. Takano : *Supercond. Sci. Technol.* **23** (2010) 054013
- 23) Z. A. Ren, G. C. Che, X. L. Dong, J. Yang, W. Lu, W. Yi, X. L. Shen, Z. C. Li, L. L. Sun, F. Zhou, and Z. X. Zhao : *Europhys. Lett.* **83** (2008) 17002.
- 24) T. Fukuda, A. Q. R. Baron, S. Shamoto, M. Ishikado, H. Nakamura, M. Machida, H. Uchiyama, S. Tsutsui, A. Iyo, H. Kito, J. Mizuki, M. Arai, H. Eisaki, and H. Hosono : *J. Phys. Soc. Jpn.* **83** (2008) 103715
- 25) Z. P. Yin, S. Lebegue, M. J. Han, B. P. Neal, S. Y. Savrasov, and W. E. Pickett : *Phys. Rev. Lett.* **101** (2008) 047001.
- 26) We note that  $x$ ,  $y$ , and  $z$  axes in our text correspond to  $X$ ,  $Y$ , and  $Z$  axes in refs. 12 and 20.
- 27) M. Rotter, M. Pangerl, M. Tegel, and D. Johrendt : *Angew. Chem. Int. Ed.* **47** (2008) 7949.
- 28) K. Horigane, H. Hiraka, and K. Ohoyama : *J. Phys. Soc. Jpn.* **78** (2009) 074718.
- 29) H. Hosono, S. Matsuishi, T. Nomura, and H. Hiramatsu : *BULLETIN* **64** (2009) 807 in Japanese.
- 30) P. C. Canfield, S. L. Bud'ko, Ni Ni, J. Q. Yan, and A. Kracher : *Phys. Rev. B* **80** (2009) 060501R.